Zn 0.35 Co 0.65 O – A Stable and Highly Active Oxygen Evolution Catalyst Formed by Zinc Leaching and Tetrahedral Coordinated Cobalt in Wurtzite Structure

Sebastian Wahl, Sayed El-refaei, Ana Guilherme Buzanich, Patrick Amsalem, Kug-seung Lee, Norbert Koch, Marie-Liesse Doublet, Nicola Pinna

$Zn_{0.35}Co_{0.65}O$ - A Stable and Highly Active Oxygen Evolution Catalyst Formed by Zinc Leaching and Tetrahedral Coordinated Cobalt in Wurtzite Structure

Sebastian Wahl,[a] Sayed M. El-Refaei,[a] Ana Guilherme Buzanich,[b] Patrick Amsalem,[c] Kug-Seung Lee,[d] Norbert, Koch,[c] Marie-Liesse Doublet[e,f], Nicola Pinna[a,]*

Affiliation

[a] Institut für Chemie and IRIS Adlershof, Humboldt-Universität zu Berlin, Brook-Taylor-Strasse 2, 12489 Berlin, Germany

[b] Bundesanstalt für Materialforschung und -prüfung (BAM), Richard-Willstätter-Straße 11, 12489 Berlin, Germany

[c] Institut für Physik and IRIS Adlershof, Humboldt-Universität zu Berlin, Brook-Taylor-Strasse 6, 12489 Berlin, Germany

[d] Beamline Department, Pohang Accelerator Laboratory, Republic of Korea

[e] Institut Charles Gerhardt, CNRS UMR5253, Université Montpellier, Place Eugène Bataillon, 34095 Montpellier, France

[f] Réseau Français sur le Stockage Electrochimique de l'Energie-RS2E, FR3459 Amiens, France

* Corresponding author email address: nicola.pinna@hu-berlin.de

Keywords

oxygen evolution reaction, cobalt, zinc, Wurtzite, γ-Co(O)OH, Structure-Property Relationships

Abstract

To arrive to sustainable hydrogen-based energy solutions, the understanding of water-splitting catalysts plays the most crucial role. Herein, we combined state-of-the-art hypotheses on electrocatalytic active metal sites towards the oxygen evolution reaction (OER) to develop a highly efficient catalyst based on earth-abundant cobalt and zinc oxides. The precursor catalyst $Zn_{0.35}Co_{0.65}O$ was synthesized via a fast microwave-assisted approach at low temperatures. Subsequent, it transformed *in situ* from the Wurtzite structure to the layered γ-Co(O)OH, while most of its zinc leaches out. This material shows outstanding catalytic performance and stability towards the OER in 1 M KOH (overpotential at 10 mA cm^{-2} $\eta_{initial}$ = 306 mV, $\eta_{98\,h}$ = 318 mV). By comparing the electrochemical results and *ex situ* analyses to today's literature, we were able to identify clear structure-activity correlations. Our findings suggest that coordinately unsaturated cobalt octahedra on the surface are indeed the active centers for the OER.

1. Introduction

In 2015, the United Nations (UN) set 17 sustainable development goals (SDGs) to be reached by 2030. Goal 7, affordable and clean energy, wants to *"Ensure access to affordable, reliable, sustainable and modern energy for all."* One target is to *"increase substantially the share of renewable energy in the global energy mix"*.[1] One approach to reach this target, is the storage of excess solar and wind energy in chemical bonding, especially in the hydrogen-hydrogen bond.[2, 3] The water splitting reaction, forming 2 H_2 and O_2 from 2 H_2O, is based on a 4 electron transfer mechanism from oxygen to hydrogen. The reaction is hindered by the half-cell reaction at the anode, the OER, which takes place at a theoretical potential of 1.23 V at standard conditions.[4] Benchmarking papers as the ones by Jaramillo et al. show periodically the best oxygen evolution catalysts (OEC).[5-7] Among those, scarce and rare ruthenium and iridium oxides are still the best performing. However, during the last years, more and more catalysts based on earth abundant

elements are registered in those benchmarks. By focusing on developing efficient water oxidation catalysts based on available metals like cobalt, nickel, manganese and iron, we come step by step closer to a large-scale realization of a circular energy economy based on hydrogen.[8]

For cobalt-based systems, it is now proven that the active site involved in the OER is based on two or more redox-active cobalt atoms changing their oxidation states from +II to +IV and back. Those are connected by μ-OH or μ-O bridges.[9, 10] A structure widely known to provide those motifs is cobalt oxyhydroxide Co(O)OH.[11-13] Pfrommer et al. have shown, that a crystalline cobalt substituted zinc oxide can yield a stable OEC in alkaline electrolyte with enhanced activity, which is on the one hand based on the amorphization of the surface and the formation of Co(O)OH.[14] On the other hand, they agreed to the findings of others, that the presence of redox-inert Zn^{2+} is "rendering structural support and/or providing cooperative effects" for the catalytically active cobalt.[15, 16] Though, what was not yet discussed there, was the dissolution/leaching of zinc from the solid materials to the solution, which is expected at the elevated *pH* values in those studies.[17-19] Correlating the leaching of Zn^{2+} into the electrolyte with an enhanced OER activity was done first, to our knowledge, by Menezes et al.[13] They examined cobalt containing spinels towards their OER activities and showed that partly leaching of Zn^{2+} from the tetrahedral sites leads to defective sites and thus increases the activity of the remaining cobalt in the octahedral sites of the spinel. Contrary to the hypothesis formed by the latter, Wang et al. studied the same system and stated, that Co^{2+} in tetrahedral sites can be easily oxidized and form Co(O)OH, which then acts as the active phase, whilst Co^{3+} in the octahedral sites is rather inactive towards the OER as it might be blocked by OH-groups.[20]

From this two opposing yet properly elaborated works, we got inspired to craft a material that combines the two identified driving forces. Thus, the material should provide a high amount of

tetrahedral coordinated cobalt, preferably in oxidation state +II, and in addition hold a sufficient amount of Zn^{2+} to be leached into the solution, leaving highly defective structures. In addition to the increase of the intrinsic activity, the material also should have a large number of accessible active sites. Inspired by Huang et al., who showed, that γ-Co(O)OH nanosheets outperform the bulk oxyhydroxide catalyst manifold and even overcome the IrO_2 catalyst, our material should exhibit also an exfoliated layered morphology .[21]

Based on our expertise on the nonhydrolytic sol-gel synthesis of transition metal oxides, particularly cobalt and zinc based, in this work we focus on the synthesis of hexagonal Zn-stabilized $Co^{II}O$ in the Wurtzite structure. This combines all of the aforementioned properties.[22-26] The synthesis involves a fast microwave-assisted solvothermal reaction of cobalt(III) acetylacetonate and zinc(II) acetate in benzyl alcohol. We analyzed the as-synthesized product thoroughly by high resolution transmission electron microscopy (HRTEM), powder X-ray diffraction (pXRD), X-ray photoelectron spectroscopy (XPS) and X-ray absorption spectroscopy (XAS). We identified the changes the sample underwent by contact with the alkaline medium by HRTEM and pXRD, and validated the findings against the available literature. Then, we characterized the catalytic performance of the *in situ* formed catalyst towards the OER by electrochemical measurements and finally derived structure/activity correlation from *ex situ*-studies.

By following this approach, we are able to provide a comprehensive study of one of the most active catalysts for the OER. The formed catalyst was able to maintain an overpotential η of less than 320 mV over a time frame of 98 h at a current density of 10 mA cm^{-2} in 1 M KOH.

2. Results and Discussion

2.1. Characterization of $Zn_{0.35}Co_{0.65}O$ precatalyst

Zinc doped hexagonal cobalt oxide was synthesized by the microwave-assisted "benzyl alcohol route". This was achieved by using cobalt(III) acetylacetonate and zinc acetate as metal precursors and benzyl alcohol as oxygen source, solvent, reducing and surface stabilizing agent.[24, 27, 28] After 20 min at 210 °C, the sample was washed with ethanol, solid products were collected by centrifugation and the sample was dried in an oven at 70 °C overnight. A dark green powdered product, denoted as $Zn_{0.35}Co_{0.65}O$, was obtained.

The crystal structure was identified by pXRD. Only typical reflections of the hexagonal Wurtzite structure (ICSD PDF-number 01-074-0534)[29] were present in the pattern in Figure 1. Shifts in the positions of the reflections are not expected, since the ionic radii for Co^{2+} and Zn^{2+} are very similar (57 vs. 60 pm) and cobalt replaces the zinc in the structure.[30, 31]

HRTEM analysis shows agglomerates of sheets that form spheres of different sizes (Figure 2 a). This is in accordance to previous work of our group and proves the trend, that a higher amount of cobalt directs the formation of spherical agglomerates.[22] Power spectra analysis of the HRTEM (Figure 2 b) shows the crystallinity of the sample, which proves the hexagonal Wurtzite structure. Energy dispersive X-ray spectroscopy (EDX) analysis yields a zinc to cobalt ratio of 0.35 to 0.65, confirming the stoichiometric implementation of both metals in the material. EDX mapping (see Figure SI-6) shows the uniform distribution of the metals in the assembly.

Insight in the oxidation state of the sample were gained by characterizing the chemical surface of the sample by XPS (Figure 3). The $Co2p_{3/2}$ peak is at 781 eV, with a shake-up satellite shifted by 5.8 eV. The $Co2p_{1/2}$ peak is shifted by 15.8 eV compared to $Co2p_{3/2}$. Comparing this to reference

compounds (see Figure SI-4 a) we can see clear difference to oxidation state +III, and from similar spectra in literature, we reason the oxidation state of cobalt is +II.[32, 33]

Further information on the oxidation state and the local atomic environment of the cobalt were provided by diffuse reflectance UV/Vis spectroscopy. The spectrum (Figure SI-3b) shows three typical absorption features at 579, 623 and 678 nm, which correspond to the transitions $^4A_2(F) \rightarrow {}^2E(G)$, $^4A_2(F) \rightarrow {}^4T_1(P)$, and $^4A_2(F) \rightarrow {}^2A_1(G)$, respectively. Those are typical for Co^{2+} in tetrahedral environment.[26, 34-36]

To access the oxidation state and the local atomic environment of cobalt X-ray absorption spectroscopy (XAS) was used. In the X-ray absorption near-edge structure spectra (XANES, Figure 4 a), the cobalt edge position in $Zn_{0.35}Co_{0.65}O$ was compared to the references $ZnCo_2O_4$ and commercially available CoO in rock salt structure.[37] The predominant cobalt oxidation state in the first reference is +III, and the edge position is 7720.6 eV ($ZnCo_2O_4$). In the second reference, the predominant oxidation state is +II, and the edge position found is 7715.8 eV. The edge position of $Zn_{0.35}Co_{0.65}O$ is at 7717.9 eV. This observation leads us to conclude, that the cobalt oxidation state in the material is less than +III, in comparison to the references. Since the pre-edge features in the XANES spectra are very prone to changes in crystal field symmetry, analysis of those also gives hints on the local structure of the absorbing atom. From the distinct pre-edge peak in the spectrum of $Zn_{0.35}Co_{0.65}O$ we deduce tetrahedral coordination of the central cobalt atom. [38]

Furthermore, we fitted the Wurtzite crystal system to the extended X-ray absorption fine structure (EXAFS) spectrum (R-range: 1.3 – 5.0, Figure 4 b), where cationic positions were filled by 65 % Co^{2+} and 35 % Zn^{2+}, derived from EDX results. The first shell around the cobalt central atom at a reduced distance of 2.0 Å contains 4 oxygen atoms. The second shell consists in a distance of

3.2 Å of 6 atoms, which are cobalt and zinc in the ratio 2:1. Overlapping with the second shell, the third shell at a distance of 3.8 Å holds 9 oxygen atoms. The signal assigned to the forth shell at 4.5 to 4.6 Å is a summation of the signals of 2 zinc, 4 cobalt and 6 oxygen atoms, as well as a multi-leg scattering part within the second and third shell. With a *R*-factor of 0.0086 for this fit, we could further confirm the tetrahedral oxygen coordination of cobalt.[39, 40] From the above mentioned analyses of the experimental data, we can safely conclude that in $Zn_{0.35}Co_{0.65}O$ cobalt is tetrahedrally coordinated and in oxidation state +II.

The homogeneity of the pre-catalyst material can be derived from the following considerations: The pXRD (Figure 1) shows only one crystalline phase, and the HRTEM micrographs exhibited only one morphology (Figure 2a). The EDX mapping (Figure SI-6) showed a uniform distribution of Zn and Co over the whole sample, and the EXAFS fit (Figure 4b) shows that the second shell consists of Zn and Co in the ratio of 1:2. Thus, the material can be described as a one phase solid solution of Wurtzite (Co/Zn)O.

2.2. Characterization of the electrochemically active structure

When $Zn_{0.35}Co_{0.65}O$ gets in contact with 1 M KOH (*pH* =13.8), it instantaneously changes color to a light brown. To figure out the origin of color change, we added some $Zn_{0.35}Co_{0.65}O$ powder to 1 M KOH and stirred the dispersion at room temperature for 90 min. Then, we washed the sample with ethanol, collected the solid products by centrifugation, and dried it in an oven at 70 °C for 1 h. The pXRD-pattern in Figure 1 shows the typical reflections of hexagonal cobalt hydroxide $Co(OH)_2$ in Brucite-type layered structure (ICSD PDF-number 01-074-1057)[41] and of hexagonal Wurtzite structure, leading to the conclusion, that the material is, at least at the surface, transformed to $Co(OH)_2$. The formation of $Co(OH)_2$ is in agreement with the findings of Jang et al., who reported that hexagonal cobalt oxide transforms spontaneously to hexagonal cobalt

hydroxide in contact with water.[42] Though, it is to mention that the incorporated Zn^{2+} seems to stabilize the structure and prevents a fast conversion. TEM micrographs of the sample show platelets of around 50 nm in diameter with a thickness of around 4 nm (Figure 2c). The EDX element ratio of cobalt to zinc is 92.6 to 7.4 %, respectively. This indicates a loss of Zn from the structure, which is addressed in detail in the following section.

Electrocatalytic activity towards the OER was examined by rotating disk electrode (RDE) measurements in 1 M KOH at 1600 rpm. Figure 5 a shows the cyclic voltammograms (CV) of $Zn_{0.35}Co_{0.65}O$ in comparison to the reference Co(O)OH (CVs for other references can be found in Figure SI-3a). In the first cycle of the CV, an intense oxidation peak at around 1.15 V is visible. This can be attributed to the oxidation of Co^{2+} to Co^{3+}, which is a further proof that the as-prepared material being in oxidation state +II. Since there is no equally sized reduction peak, we conclude an irreversible oxidation event. From the pXRD results we know that $Co(OH)_2$ is formed *in situ*. It has been described for other $Co(OH)_2$ systems, that this peak can be attributed to the irreversible oxidation of $Co(OH)_2$ to the cobalt oxyhydroxide Co(O)OH.[43-45] In the 4th CV cycle, 2 oxidation/reduction pairs are visible, slightly above 1.0 V and around 1.4 V. They can be assigned to the reversible oxidation of $Co^{2+/3+}$ and $Co^{3+/4+}$, respectively. From the higher current density of $Zn_{0.35}Co_{0.65}O$ compared to the references, we conclude there are more accessible cobalt sites. To determine the electrochemically active surface area (ECSA), we used the method described by McCrory and measured the double-layer capacitance (see Figure SI-2).[7] We found that the ECSA was around 20-fold larger than for the reference catalysts. This is as well in very good agreement with the TEM observation of exfoliated layered structures.

Monitoring the electrocatalytic performance of $Zn_{0.35}Co_{0.65}O$ compared to other cobalt containing catalysts in linear sweep voltammetry, it shows on the one hand a larger deviation between single

measurements than the other catalysts. On the other hand, it has a significantly decreased average overpotential η of 322 mV compared to 365 mV for Co_3O_4, 369 mV for $ZnCo_2O_4$ and CoO, respectively, and 382 mV for Co(O)OH at a current density of 10 mA cm^{-2} (Figure 5 d). The high activity is also reinforced by the low Tafel slope of 42.6 mV dec^{-1} (Table 1). Comparison of Tafel slopes shows that all reactions take place in the same kinetic regime around 40 mV dec^{-1} within a 10 mV dec^{-1} window. The examined materials have the same rate-determining step in the region where the Tafel slope was calculated. According to Shinagawa et al., the rate-determining step in this Tafel region could be either assigned to a high coverage of the low-coordinated surface metal centers by OH^- species or to a high coverage of the surface with *OOH species.[46] Therefore, in the present article the Tafel slopes are provided for comprehensiveness of the electrochemical analyses, the in depth analysis of those is beyond the scope of this work.

To evaluate the long-term stability of the catalyst, we tracked the potential response in a chronopotentiometric measurement at a current density of 10 mA cm^{-2} on an Au-electrode. During 98 h, the potential increased linearly from 1.534 to 1.546 V vs. RHE, which corresponds to an overpotential η of 306 to 318 mV. Linear fitting of the data resulted in a mean potential increase of 0.12 mVh^{-1}. By this, we were able to prove the long-term stability of our material (Figure 5 c).

2.3. Characterization of the material after electrolysis

After 1 h electrochemical reaction at a current density of 10 mA cm^{-2}, XPS measurements were performed directly on the screen printed electrode (Figure 3). The peaks of $Co2p_{3/2}$ and $Co2p_{1/2}$ are shifted to lower binding energies of 779.9 eV and 795.0 eV, respectively. Also, the first shake-up satellite is shifted by 10.0 eV towards lower energies (Figure 3a). From this, we deduce a change in oxidation state to +III. [32, 33, 47] The biggest change though is visible at the zinc edge.

Before the reaction the peaks for zinc were clearly observable, but after the reaction there is no more signal (Figure 3b). In alkaline media, ZnO first reacts to the insoluble $Zn(OH)_2$. With an excess of hydroxide, the soluble $[Zn(OH)_4]^{2-}$ complex is then formed.[19] This indicates the leaching of Zn^{2+} from the surface during the reaction.

In the pXRD pattern (Figure 1), three main reflections are visible. At *2 θ* angles of 5.57, 16.7 and 28.76 °, those reflections correspond to d-values of 7.3, 2.44 and 1.43 Å, respectively. Comparing this values to the ones reported by Bardé et al., we can assign the reflections to the (003), (101) and (110) lattice planes of a slightly distorted γ-Co(O)OH.[48] From the Bragg reflection broadening, we derive a poor crystallinity of the oxyhydroxide. The asymmetric reflections of the (101) and (110) indicate a turbostratic disorder of the basal planes.[49] The *d*-value of 7.3 Å of the (003) lattice plane can be directly translated to the interlayer distance of the material.

The TEM micrograph of the sample after electrochemical characterization in Figure 2 (d) shows the main motifs are still layers, agglomerated to spheres. In contrast to the original sample, those layers are more exfoliated and the spheres are less separated from each other. Selected area electron diffraction of a large area (Figure 2 (e) shows weak Debye-Scherrer rings corresponding to interplanar distances of 2.42 and 1.44 Å, matching well the results of our pXRD analysis as well as the TEM analysis by Huang et al.[21] Here, it is to mention, that the sample is beam-sensitive, which is in agreement with the reported recrystallization of Ni(O)OH under an electron beam (see SI for more information).[50]

In contrast to the XPS measurements, where no zinc was detected on the materials surface, in EDX measurements 2.6 up to 6.5 atm.-% of zinc were detected (Table 2). Noteworthy, the amount of zinc decreased towards the edge of particle agglomerations (see Figure SI-8).

Analyzing the EDX mapping in figure 6, no such trend can be seen. Cobalt and oxygen are well dispersed over the whole structure. Due to the low abundance of the zinc in the sample, there are no areas detectable, where a position/zinc concentration correlation could be drawn. Only a uniform distribution of zinc in the examined structure can be seen. The high angle annular dark field (HAADF) micrograph in the same figure also shows the layered motifs as the bright field image. Although the shown agglomerate has a width of around 200 nm, the low phase contrast all over the agglomerate indicates a material of low density and high surface. A clear attribution of areas with higher Zn or Co content is not possible in the HAADF, as the electron density of the two elements is nearly the same.

From the XANES edge position at 7721.2 eV (Figure 4a), we deduce a predominant oxidation state of +III or slightly above in the sample after the electrochemical reaction. The distinct pre-edge feature indicates a non-symmetric geometry around the cobalt absorber. The EXAFS spectrum in Figure 4b clearly differs from the one before the reaction. The spectrum was fitted in the R-range from 1.0 to 3.5 Å by fixing the amplitude reduction factor S_0^2 to a value determined prior, as described by Ravel and Kelly.[51] Thus, the degeneracies of the $Zn_{0.35}Co_{0.65}O$ after 1 h electrochemical reaction could be obtained. For a single-scatterer, the degeneracy equals the coordination number. The fit of the first three shells of $Zn_{0.35}Co_{0.65}O$ after 1 h of electrochemical reaction was based on the hexagonal Co(O)OH structure without any dopant. The first shell around the absorbing Co-atom contains 5.6 O-atoms in a reduced distance of 1.91 Å. The second shell consists of 4.6 Co-atoms in a distance of 2.84 Å. The third shell holds 4.3 O-atoms in a distance of 3.44 Å. With an *R*-factor of 0.012, the fit indicates oxygen vacancies in the first shell and metal-ion vacancies in the second shell.

2.4. Structure-activity correlations

Detection of $Co(OH)_2$ and Wurtzite crystal structures after 90 min in 1 M KOH is in contrast to the previously reported rapid total conversion of hexagonal CoO and points to a stabilizing influence of Zn.[42] It further proves that $Co(OH)_2$ is an important intermediate in the electrochemical formation of γ-Co(O)OH.

To explain the high activity of $Zn_{0.35}Co_{0.65}O$ towards the OER, structure factors can be compared to reference-samples, thoroughly described in the literature. For all those samples, it is agreed that the OER activity arises from adjacent $Co^{(III-IV)}O(H)$ groups connected by μ_2-O-bridges.[10, 11, 52] The leaching of Zn^{2+} in alkaline media leads to increased metal vacancies in the material, as proven by the EXAFS analysis of the sample after electrochemical reaction. The second coordination shell consists only of 4.6 metal atoms instead of 6.0. Comparable results were published by Menezes et al, who analyzed the leaching of Zn^{2+} from the cubic spinel $ZnCo_2O_4$.[13] They conclude, that by leaching of Zn^{2+}, more octahedral Co^{3+} sites are accessible compared to Co_3O_4, and that tetrahedral voids favor the restructuring of the surface. To compare $Zn_{0.35}Co_{0.65}O$ to their results, we synthesized $ZnCo_2O_4$. We also observed the dissolution of Zn^{2+} from the spinel (see SI for detailed description), but in contrast to their work, we found the Zn^{2+}-containing spinel oxide performed worse than the Co_3O_4 reference. This finding is supported by the work of Wang et al, that compared $CoAl_2O_4$, Co_3O_4 and $ZnCo_2O_4$ towards their OER activity.[20] They concluded, that Co^{3+} fully coordinated by 6 O(H) groups is mostly inaccessible for taking part in the OER. Our comparison to other cobalt oxides that are constructed of CoO_6 building blocks, namely CoO in rock-salt structure and Co(O)OH, shows similar results. Their activity is decreased compared to Co_3O_4 and $Zn_{0.35}Co_{0.65}O$. Further proof of this theory is also given by our observation, that Co(O)OH has the second highest ECSA, roughly five-fold higher

than the other references, but the lowest OER activity. Thus, we deduct from our findings, that solely a higher accessibility of CoO_6 is not the reason for a high OER activity.

Instead, when starting from tetrahedral coordinated Co and transforming it to octahedral Co, O-vacancies and coordinately unsaturated $CoO_{(6-x)}$-motifs are introduced in the structure.[20] EXAFS analysis shows, that the oxygen coordination number is decreased to 5.6 instead of 6.0 in the first coordination shell. By this, as proven by density of states (DOS) studies by others on $CoO_{(6-x)}$-motifs on the surface of γ-Co(O)OH, the DOS near the Fermi level is increased. Thus, higher conductivity is achieved, which favors the electron transport from the active site.[21] Nevertheless, the extraction of Zn^{2+} from the surface also contributes to the change of the electronic structure. Co and O undergo an oxidation process and arrive to a higher valence.[53, 54] Thus, the electrophilicity of surface-O can increase, which leads to a faster adsorption of OH^- to form the *OOH species, which is the rate determining step, which is also in accordance to the calculated Tafel slope. In addition to this, it is nowadays accept that a lower overpotential is correlated to a higher adsorption stabilization energy of *OOH compared to *OH.[55-58] The remaining few percent of Zn^{2+} in the structure play also an important role for the conductivity of the sample. Ling et al. have recently shown, how 4-6 atm.-% of Zn in CoO can greatly enhance the ionic diffusion and electronic conductivity though the material.[59] Another contribution to higher conductivity might be also chemical bonding of the active material to the conducting support, obtained by the *in situ* formation of the active phase.[16, 42] One more attribution to the increased OER activity, beside the above mentioned intrinsic factors, is the overall higher number of accessible cobalt sites.[60, 61] The accessibility of those cobalt sites is further raised by the slightly enlarged inter-layer-distance of 7.3 Å in our γ-Co(O)OH.[21, 43, 60]

3. Conclusion

The successful synthesis of $Zn_{0.35}Co_{0.65}O$ can connect this work to previous studies of our group on the field of cobalt-doped zinc oxides in Wurtzite structure by the non-hydrolytic benzyl alcohol route.[22] Herein, we report a fast, easy and reproducible one-pot synthesis for a zinc-stabilized cobalt oxide that, by its exfoliated morphology, acts as an excellent precursor catalyst for the OER.

In an alkaline solution with an applied anodic potential, the material undergoes structural transformation to γ-Co(O)OH: Edge-sharing octahedra are formed and act as the active site. A high defect concentration induced by the leaching of Zn^{2+} and the structural transformation eases the accessibility of those active centers. Thus, an optimized energetic stabilization of the *OOH species, whose formation is the rate determining step, is achieved. Furthermore, the number of active sites is increased by the presence of exfoliated layers which provide a high surface area. This leads to an exceptional activity for the OER, with an overpotential η of 306 mV at a current density of 10 mA cm^{-2}. During 98 h at the same current density, the overpotential just increased by 12 mV, proving the stability of the *in situ* formed catalyst. Further works should focus on different leaching agent and the optimal ratio of catalyst/leaching agent.

In summary, we could unify two contradicting hypotheses,[13, 20] and we experimentally derived structure-activity correlations in a catalyst based solely on earth-abundant zinc and cobalt oxides. Finally, by showing a high stability besides a high activity, our work possesses high potential to play a key-role in a sustainable hydrogen powered future.

4. Experimental

4.1. Materials

All reagents were used as received. Cobalt(III) acetylacetonate (98%) and cobalt(II) oxide (99.995%, metal basis; denoted as commercial CoO) were purchased from ABCR GmbH (Karlsruhe, Germany). 1 N potassium hydroxide solution was purchased from Carl Roth GmbH (Karlsruhe, Germany). Benzyl alcohol (99%), Nafion perfluorinated resin solution (5 wt-%) and zinc(II) acetate (99.99%) were purchased from Sigma Aldrich (Munich, Germany). Purified water with resistivity 18.2 $M\Omega cm^{-1}$ was used for sample preparation.

4.2. Syntheses

$Co_{0.65}Zn_{0.35}O$ was synthesized by adding cobalt(III) acetylacetonate (71 mg, 0.2 mmol, 2 eq.) and zinc acetate (18 mg , 0.1 mmol, 1 eq.) to benzyl alcohol (3 mL) in a 10 mL microwave reaction vial. The reaction mixture was stirred at room temperature for 2 h, until all precursors were dissolved. Subsequently, the mixture was heated in a microwave reactor (CEM Discover SP, Kamp-Lintfort, Germany) at 60 °C for 2 min followed by 210 °C for 20 min, and cooled down rapidly with compressed air. The solid product was collected by centrifugation, washed three times with ethanol and dried overnight at 70 °C. Averaged over 6 reaction, the yield was 18.8 mg of a dark green product (81.5 % yield on precursor's stoichiometry).

Syntheses of the reference catalysts can be found in the supporting information.

4.3. Characterization

Powder X-Ray diffraction patterns were obtained using a STOE STADI MP (STOE, Darmstadt, Germany) running at U = 40 kV and I = 40 mA with Mo Kα = 0.70930 Å) monochromatic radiation (using a Ge(111) monochromator) and a DECTRIS "MYTHEN 1K" detector. The patterns were recorded in *2 θ* geometry in the range of 4 to 60 °.

High resolution transmission electron microscopy (HRTEM) images were obtained using a FEI Talos F200S operated at 200 kV scanning/transmission electron microscope (S/TEM). Energy dispersive X-ray spectra (EDX) and maps were recorded with build in SuperX EDS detector. EDX spectra were analyzed using FEI TEM Imaging & Analysis software version 4.17 SP1. EDX mappings were analyzed using FEI Velox software version 2.6 with the Schreiber-Wims ionization cross-section model. The errors reported are taken from the reports generated by the software.

The XANES and EXAFS measurements of the samples before electrochemical reaction were performed at the BAM*line* (BESSY-II, Helmholtz Centre Berlin for Materials and Energy Berlin, Germany). The beam was monochromatized using a double-crystal monochromator (DCM). The size of the beam was 3 x 1 mm. The measurements were performed at Co-K edge (7709 eV) in transmission geometry, with two ionization chambers as detectors. The excitation energy was varied from 7614 eV to 8428 eV, with varying energy steps. For the pre-edge region, the energy was varied in 10 eV steps; for the region around the edge, energy was tuned in 0.5 eV steps and in the EXAFS region with a constant step in the k-space of 0.04 $Å^{-1}$. The associated uncertainty was experimentally determined by measuring the cobalt metal foil 10 times. A value of ±0.3 eV was obtained. For the measurement, the samples were mixed with boron nitride and fixed in plastic sample holders. Before collecting the sample spectra, a cobalt foil was used as a reference for the cobalt edge. The relative energies of the spectra were calibrated to the first infliction point of the cobalt metal absorption edge. XANES and EXAFS measurement of the sample after 1 h electrochemical reaction on a gold screen printed electrode (DropSense 250AT, Metrohm, Filderstadt, Germany) were measured at 8C nano-probe XAFS beamline (BL8C) of Pohang Light Source (PLS-II) in the 3.0 GeV storage ring, with a ring current of 400 mA. The X-ray beam was monochromated by a Si(111) double crystal where the beam intensity was reduced by 30% to

eliminate the higher-order harmonics. The x-ray beam was then delivered to a secondary source aperture where the beam size was adjusted to be 0.5 mm (v) × 1 mm (h). XAFS spectra were collected in fluorescence mode. To determine the edge energy, the integral-method was used.[37] EXAFS data were processed by ATHENA and ARTEMIS from Demeter version 0.9.26.[39] This GUIs program belongs to the main package IFEFFIT (v. 1.2.12).[62]

X-ray photoelectron spectroscopy (XPS) was performed in an ultrahigh vacuum chamber (base pressure 5.10-10 mbar) using a JEOL JPS-9030 set-up comprising a hemispherical photoelectron spectrometer and a monochromatic Al Kα (hν = 1486.6 eV) X-ray source. The XPS measurements were performed with an energy resolution of 0.7 eV as determined on a polycrystalline Ag *3d* core level.

4.4. *Electrochemical analyses*

Electrochemical analyses were performed using a Bio-Logic VMP3 multichannel potentiostat/ galvanostat with a built-in EIS analyzer. The electrochemical behavior and activity of catalysts were measured in a three-electrode electrochemical cell using a 3 mm diameter glassy carbon rotating disc electrode (RDE, Autolab RRDE, Metrohm, Filderstadt, Germany) operated at 1600 rpm at 25 °C. A platinum wire was used as the counter electrode and a reversible hydrogen electrode (HydroFlex, gaskatel, Kassel, Germany) was used as a reference electrode. The electrodes were prepared by drop casting 3 µL of a catalyst ink onto glassy carbon. The ink was prepared by sonicating 1 mg catalyst powder with 490 µL ethanol, 490 µL purified water and 20 µL Nafion for 30 min.

The sample for the TEM and pXRD analyses was prepared by dropcasting an ethanolic dispersion of the catalyst onto a nickel foil, performing 1 h chronopotentiometry at a current

density of 10 mA cm^{-2}, rinsing the foil with ethanol and scratching off the material. This was repeated several times.

Long-term stability tests were performed on screen printed electrodes (DropSense 250AT, Metrohm, Filderstadt, Germany) consisting of a gold working electrode with a diameter of 4 mm and a platinum counter electrode. A reversible hydrogen electrode (HydroFlex, gaskatel, Kassel, Germany) was used as the reference electrode. 2 µL of an ethanolic dispersion (5 mg/mL) of the catalyst were dropcasted on the gold electrode and dried in an air stream. Then, the electrode was placed in 150 mL of a 1 M KOH solution at room temperature, a current of 1.257mA was applied for 98 h (1 h for XPS measurement) and the potential was recorded every 0.5 s.

4.5. *Electrocatalytically active surface area (ECSA)*

The *ECSA* was determined by double-layer capacitance (C_{dl}) measurements in 1 M KOH. Therefor, 5 cyclic voltammograms at each scan rate (10, 20, 30, 40, 50, 60, 80 and 100 mVs^{-1}) were measured in the non-Faradaic region, which is a 100 mV potential window around the open circuit voltage of the system. For the last 4 cycles of each scan rate, the anodic and the cathodic currents at the open circuit voltage were averaged and plotted versus the scan rate. By applying linear fits to these and averaging the absolute slopes of the fits, C_{dl} is calculated. The *ECSA* is C_{dl} divided by the general specific capacitance C_s, which is typically reported as 0.040 $mFcm^{-2}$ in 1 M alkaline media. The origin of this value is discussed in depth in the supplementary information of the 2013 benchmarking paper of Charles C. L. McCrory.[7] To calculate the roughness R_f, the *ECSA* is divided by the geometric area of the electrode.

5. Acknowledgement

Special thanks to Christoph Erdmann for measuring HRTEM and S/TEM.

6. References

[1] United Nations, *Resolution adopted by the General Assembly* **2015**.

[2] J. O. M. Bockris, *Int. J. Hydrogen Energy* **2002**, *27*, 731-740.

[3] Z. W. Seh, J. Kibsgaard, C. F. Dickens, I. Chorkendorff, J. K. Nørskov, T. F. Jaramillo, *Science* **2017**, *355*, eaad4998.

[4] H. Dau, C. Limberg, T. Reier, M. Risch, S. Roggan, P. Strasser, *ChemCatChem* **2010**, *2*, 724-761.

[5] S. Jung, C. C. McCrory, I. M. Ferrer, J. C. Peters, T. F. Jaramillo, *J. Mater. Chem. A* **2016**, *4*, 3068-3076.

[6] C. C. McCrory, S. Jung, I. M. Ferrer, S. M. Chatman, J. C. Peters, T. F. Jaramillo, *J. Am. Chem. Soc.* **2015**, *137*, 4347-4357.

[7] C. C. McCrory, S. Jung, J. C. Peters, T. F. Jaramillo, *J. Am. Chem. Soc.* **2013**, *135*, 16977-16987.

[8] L. Han, S. Dong, E. Wang, *Adv. Mater.* **2016**, *28*, 9266-9291.

[9] M. Risch, F. Ringleb, M. Kohlhoff, P. Bogdanoff, P. Chernev, I. Zaharieva, H. Dau, *Energy Environ. Sci.* **2015**, *8*, 661-674.

[10] A. Bergmann, T. E. Jones, E. M. Moreno, D. Teschner, P. Chernev, M. Gliech, T. Reier, H. Dau, P. Strasser, *Nat. Catal.* **2018**, *1*, 711.

[11] M. Zhang, M. De Respinis, H. Frei, *Nat. Chem.* **2014**, *6*, 362.

[12] L. Trotochaud, J. K. Ranney, K. N. Williams, S. W. Boettcher, *J. Am. Chem. Soc.* **2012**, *134*, 17253-17261.

[13] P. W. Menezes, A. Indra, A. Bergmann, P. Chernev, C. Walter, H. Dau, P. Strasser, M. Driess, *J. Mater. Chem. A* **2016**, *4*, 10014-10022.

[14] J. Pfrommer, M. Lublow, A. Azarpira, C. Göbel, M. Lücke, A. Steigert, M. Pogrzeba, P. W. Menezes, A. Fischer, T. Schedel-Niedrig, *Angew. Chem.* **2014**, *126*, 5283-5287.

[15] X. Zou, A. Goswami, T. Asefa, *J. Am. Chem. Soc.* **2013**, *135*, 17242-17245.

[16] X. Liu, Z. Chang, L. Luo, T. Xu, X. Lei, J. Liu, X. Sun, *Chem. Mater.* **2014**, *26*, 1889-1895.

[17] J. Han, W. Qiu, W. Gao, *J. Hazard. Mater.* **2010**, *178*, 115-122.

[18] S.-W. Bian, I. A. Mudunkotuwa, T. Rupasinghe, V. H. Grassian, *Langmuir* **2011**, *27*, 6059-6068.

[19] G. Jander, E. Blasius, *Lehrbuch der analytischen und praparativen anorganischen Chemie*, 14 ed., S. Hirzel, Stuttgart, **1995**.

[20] H.-Y. Wang, S.-F. Hung, H.-Y. Chen, T.-S. Chan, H. M. Chen, B. Liu, *J. Am. Chem. Soc.* **2015**, *138*, 36-39.

[21] J. Huang, J. Chen, T. Yao, J. He, S. Jiang, Z. Sun, Q. Liu, W. Cheng, F. Hu, Y. Jiang, *Angew. Chem. Int. Ed.* **2015**, *54*, 8722-8727.

[22] X. Han, S. Wahl, P. A. Russo, N. Pinna, *Nanomaterials* **2018**, *8*, 249.

[23] N. Pinna, *J. Mater. Chem.* **2007**, *17*, 2769-2774.

[24] N. Pinna, M. Niederberger, *Angew. Chem. Int. Ed.* **2008**, *47*, 5292-5304.

[25] M. H. Oh, T. Yu, S.-H. Yu, B. Lim, K.-T. Ko, M.-G. Willinger, D.-H. Seo, B. H. Kim, M. G. Cho, J.-H. Park, K. Kang, Y.-E. Sung, N. Pinna, T. Hyeon, *Science* **2013**, *340*, 964-968.

[26] G. Clavel, M.-G. Willinger, D. Zitoun, N. Pinna, *Adv. Funct. Mater.* **2007**, *17*, 3159-3169.

[27] I. Bilecka, I. Djerdj, M. Niederberger, *Chem. Commun.* **2008**, 886-888.

[28] K. M. Nam, J. H. Shim, D.-W. Han, H. S. Kwon, Y.-M. Kang, Y. Li, H. Song, W. S. Seo, J. T. Park, *Chem. Mater.* **2010**, *22*, 4446-4454.

[29] S. Abrahams, J. Bernstein, *Acta Crystallogr. B* **1969**, *25*, 1233-1236.

[30] R. T. Shannon, C. T. Prewitt, *Acta Crystallogr. B* **1969**, *25*, 925-946.

[31] R. t. Shannon, C. Prewitt, *Acta Crystallogr. B* **1970**, *26*, 1046-1048.

[32] J. Yang, H. Liu, W. N. Martens, R. L. Frost, *J. Phys. Chem. C* **2010**, *114*, 111-119.

[33] M. C. Biesinger, B. P. Payne, A. P. Grosvenor, L. W. M. Lau, A. R. Gerson, R. S. C. Smart, *Appl. Surf. Sci.* **2011**, *257*, 2717-2730.

[34] J. Hays, K. Reddy, N. Graces, M. H. Engelhard, V. Shutthanandan, M. Luo, C. Xu, N. Giles, C. Wang, S. Thevuthasan, *Journal of Physics: Condensed Matter* **2007**, *19*, 266203.

[35] D. A. Schwartz, N. S. Norberg, Q. P. Nguyen, J. M. Parker, D. R. Gamelin, *J. Am. Chem. Soc.* **2003**, *125*, 13205-13218.

[36] H. A. Weakliem, *J. Chem. Phys.* **1962**, *36*, 2117-2140.

[37] H. Dau, P. Liebisch, M. Haumann, *Analytical and Bioanalytical Chemistry* **2003**, *376*, 562-583.

[38] T. E. Westre, P. Kennepohl, J. G. DeWitt, B. Hedman, K. O. Hodgson, E. I. Solomon, *J. Am. Chem. Soc.* **1997**, *119*, 6297-6314.

[39] B. Ravel, M. Newville, *J. Synchrotron Radiat* **2005**, *12*, 537-541.

[40] S. Calvin, *XAFS for Everyone*, CRC press, **2013**.

[41] W. Lotmar, W. Feitknecht, *Kristallogr. Cryst. Mater* **1936**, *93*, 368.

[42] K. Y. Jang, G. Park, K. H. Oh, J. H. Seo, K. M. Nam, *Chem. Commun.* **2017**, *53*, 4120-4123.

[43] M. S. Burke, M. G. Kast, L. Trotochaud, A. M. Smith, S. W. Boettcher, *J. Am. Chem. Soc.* **2015**, *137*, 3638-3648.

[44] R. D. L. Smith, M. S. Prévot, R. D. Fagan, S. Trudel, C. P. Berlinguette, *J. Am. Chem. Soc.* **2013**, *135*, 11580-11586.

[45] J. A. Koza, C. M. Hull, Y.-C. Liu, J. A. Switzer, *Chem. Mater.* **2013**, *25*, 1922-1926.

[46] T. Shinagawa, A. T. Garcia-Esparza, K. Takanabe, *Scientific Reports* **2015**, *5*, 13801.

[47] B. J. Tan, K. J. Klabunde, P. M. Sherwood, *J. Am. Chem. Soc.* **1991**, *113*, 855-861.

[48] F. Bardé, M.-R. Palacin, B. Beaudoin, A. Delahaye-Vidal, J.-M. Tarascon, *Chem. Mater.* **2004**, *16*, 299-306.

[49] M. Rajamathi, P. V. Kamath, R. Seshadri, *Mater. Res. Bull.* **2000**, *35*, 271-278.

[50] K. W. Kwan, D. Xie, R. Zhang, Z. Shan, A. H. Ngan, *Phys. Status Solidi A* **2018**.

[51] B. Ravel, S. Kelly, in *AIP Conference Proceedings, Vol. 882*, AIP, **2007**, pp. 150-152.

[52] M. Favaro, J. Yang, S. Nappini, E. Magnano, F. M. Toma, E. J. Crumlin, J. Yano, I. D. Sharp, *J. Am. Chem. Soc.* **2017**, *139*, 8960-8970.

[53] L. Dahéron, R. Dedryvere, H. Martinez, M. Ménétrier, C. Denage, C. Delmas, D. Gonbeau, C*hem. Mater.* **2007**, *20*, 583-590.

[54] S.-F. Hung, Y.-T. Chan, C.-C. Chang, M.-K. Tsai, Y.-F. Liao, N. Hiraoka, C.-S. Hsu, H. M. Chen, *J. Am. Chem. Soc.* **2018**, *140*, 17263-17270.

[55] Z. Lu, H. Wang, D. Kong, K. Yan, P.-C. Hsu, G. Zheng, H. Yao, Z. Liang, X. Sun, Y. Cui, *Nat. Commun.* **2014**, *5*, 4345.

[56] J. Suntivich, K. J. May, H. A. Gasteiger, J. B. Goodenough, Y. Shao-Horn, *Science* **2011**, *334*, 1383-1385.

[57] B. S. Yeo, A. T. Bell, *J. Am. Chem. Soc.* **2011**, *133*, 5587-5593.

[58] B. Zhang, X. Zheng, O. Voznyy, R. Comin, M. Bajdich, M. García-Melchor, L. Han, J. Xu, M. Liu, L. Zheng, F. P. García de Arquer, C. T. Dinh, F. Fan, M. Yuan, E. Yassitepe, N. Chen, T. Regier, P. Liu, Y. Li, P. De Luna, A. Janmohamed, H. L. Xin, H. Yang, A. Vojvodic, E. H. Sargent, *Science* **2016**, *352*, 333-337.

[59] T. Ling, P. Da, X. Zheng, B. Ge, Z. Hu, M. Wu, X.-W. Du, W.-B. Hu, M. Jaroniec, S.-Z. Qiao, *Science Advances* **2018**, *4*, eaau6261.

[60] W. T. Hong, M. Risch, K. A. Stoerzinger, A. Grimaud, J. Suntivich, Y. Shao-Horn, *Energy Environ. Sci.* **2015**, *8*, 1404-1427.

[61] K. A. Stoerzinger, L. Qiao, M. D. Biegalski, Y. Shao-Horn, *J. Phys. Chem. Lett.* **2014**, *5*, 1636-1641.

[62] M. Newville, *J. Synchrotron Radiat* **2001**, *8*, 322-324.

[63] R. G. Delaplane, J. A. Ibers, J. R. Ferraro, J. J. Rush, *J. Chem. Phys.* **1969**, *50*, 1920-1927.

7. Figures

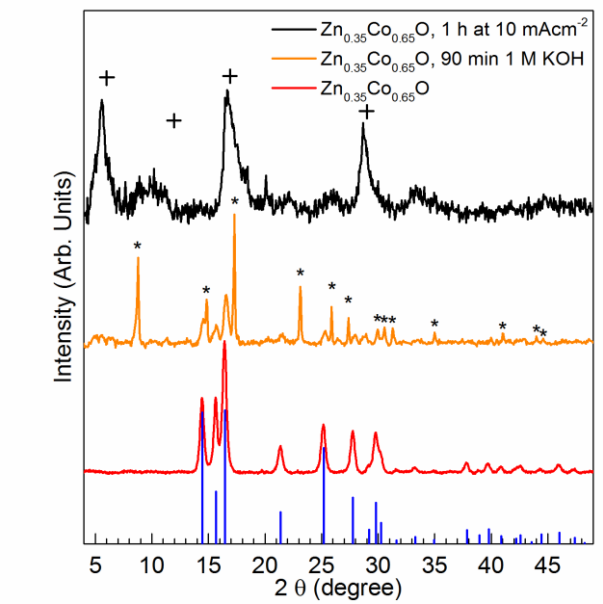

Figure 1. pXRD patterns of as prepared $Zn_{0.35}Co_{0.65}O$ (red), product after 90 min stirring in 1 M KOH (orange) and product collected after 1 h Chronopotentiometry at 10 mA cm^{-2}. References given are hexagonal Wurtzite structure (blue, ICSD PDF-number 01-074-0534), hexagonal $Co(OH)_2$ (asterisks, ICSD PDF-number 01-074-1057) and hexagonal γ-Co(O)OH (crosses, Barde et al.). [29, 41, 48]

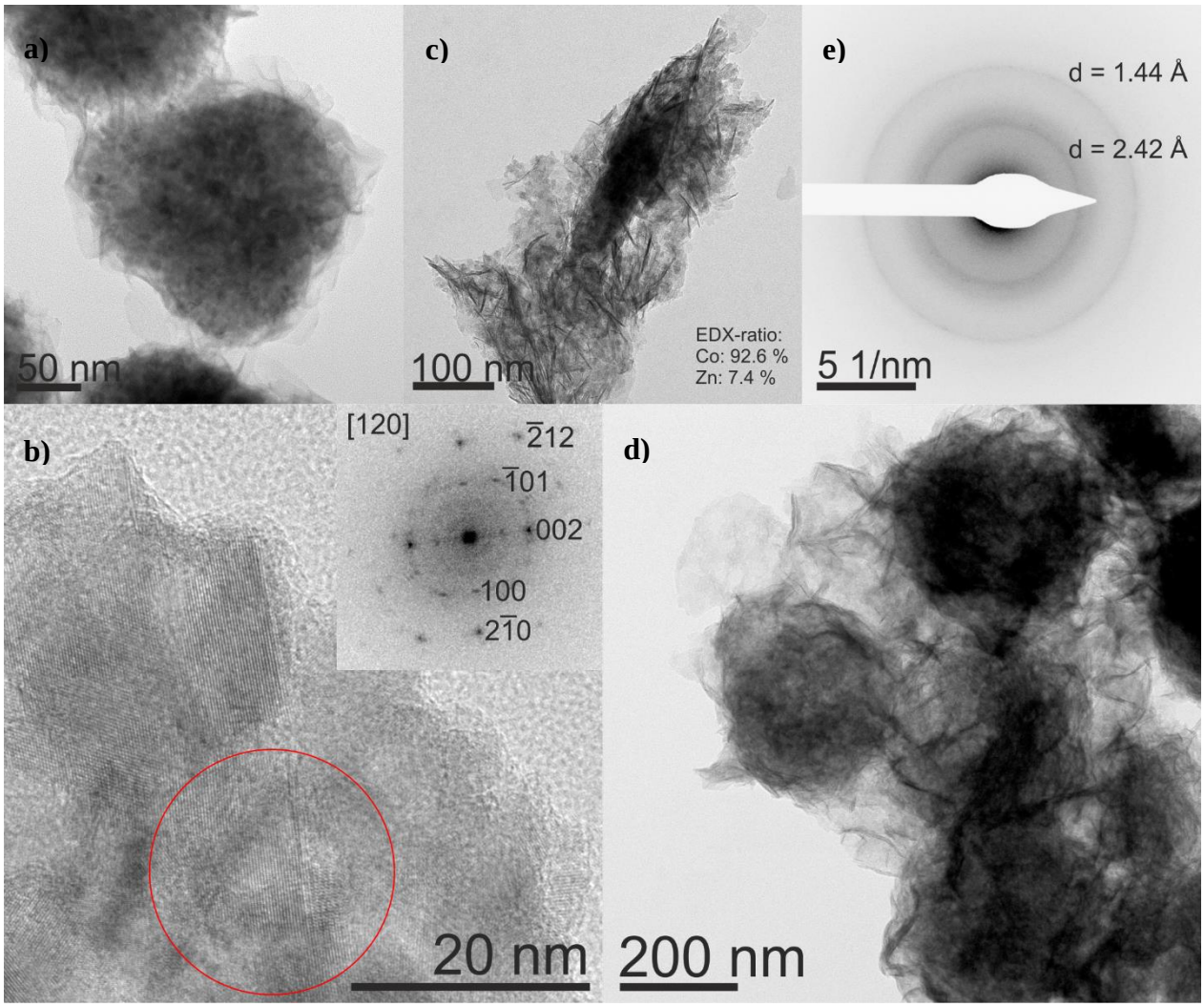

Figure 2. HRTEM micrographs of $Zn_{0.35}Co_{0.65}O$: Sample before the electrochemical reaction (a and b). The sample consists of layers that agglomerates to form spheres of different sizes (a). HR-micrograph of the edge of a sphere (b). The inset shows the power spectrum of the area selected by the red circle. The spots can be assigned to a hexagonal Wurtzite structure aligned along the [120] zone axis. The sample after 90 min in 1 M KOH consists of platelets with a thickness around 4 nm and a diameter of around 50 nm (c). The sample after 1 h electrochemical reaction at a current density of 10 mA cm^{-2} (d and e). The main motifs are still layers agglomerated to spheres, but more exfoliated and less separated than before (d). The SAED of c shows diffractions that have *d*-spaces of 2.42 and 1.44 Å (e).

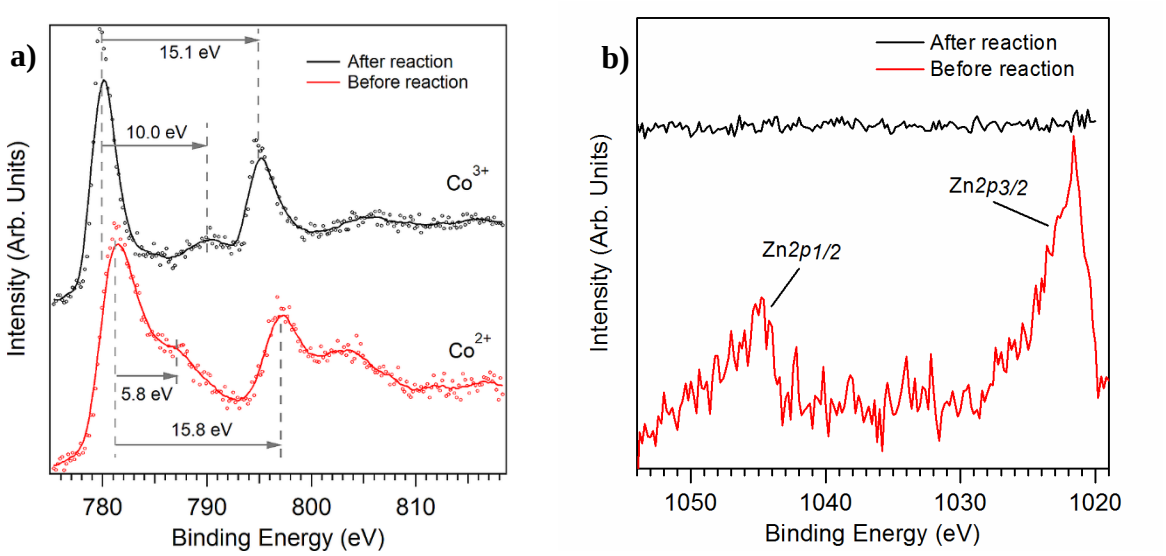

Figure 3. ex situ XPS on cobalt edge of $Zn_{0.35}Co_{0.65}O$ sample before (red) and after (black) electrochemical reaction: Before the reaction, the peak position and relative energy shifts on the cobalt edge tend to an oxidation state of +II; after the reaction, the peak positions as well as the chemical shift of the shake-up satellites lead to the conclusion the materials oxidation state has changed to +III (a). On the zinc edge, the missing Zn peak after the reaction indicates the leaching of Zn in the solution (b).

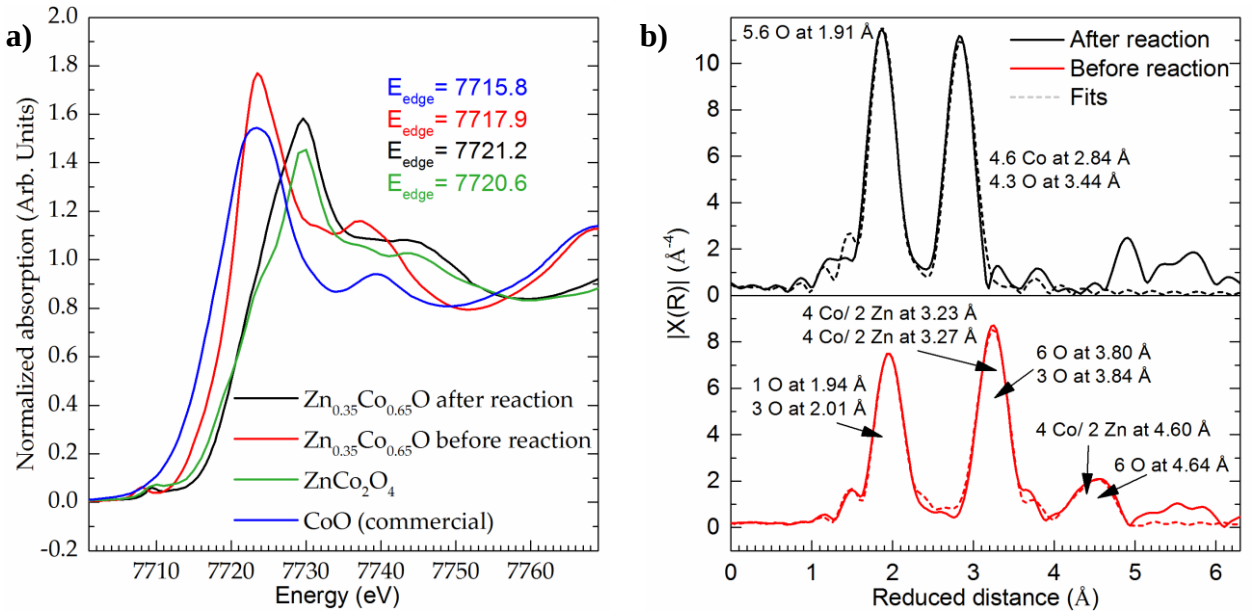

Figure 4. XAS on cobalt as absorbing atom; XANES spectra edge positions lie at 7720.6 eV ($ZnCo_2O_4$), 7721.2 eV ($Zn_{0.35}Co_{0.65}O$ after reaction) and 7717.9 eV ($Zn_{0.35}Co_{0.65}O$ before reaction. Commercially available CoO in rock salt structure was added as a reference for Co^{2+} (a). EXAFS spectra and fits of $Zn_{0.35}Co_{0.65}O$ before and after 1 h in 1 M KOH at a current density of 10 mA cm^{-2}. The fit of the spectrum before the reaction (R-range: 1.3 – 5.0 Å) is based on hexagonal Wurtzite crystal structure. The fit of the spectrum after the reaction (R-range: 1.0 – 3.5 Å) is based on hexagonal Co(O)OH in layered Brucite structure.[33, 63] The insets show the assigned surrounding atoms (b).

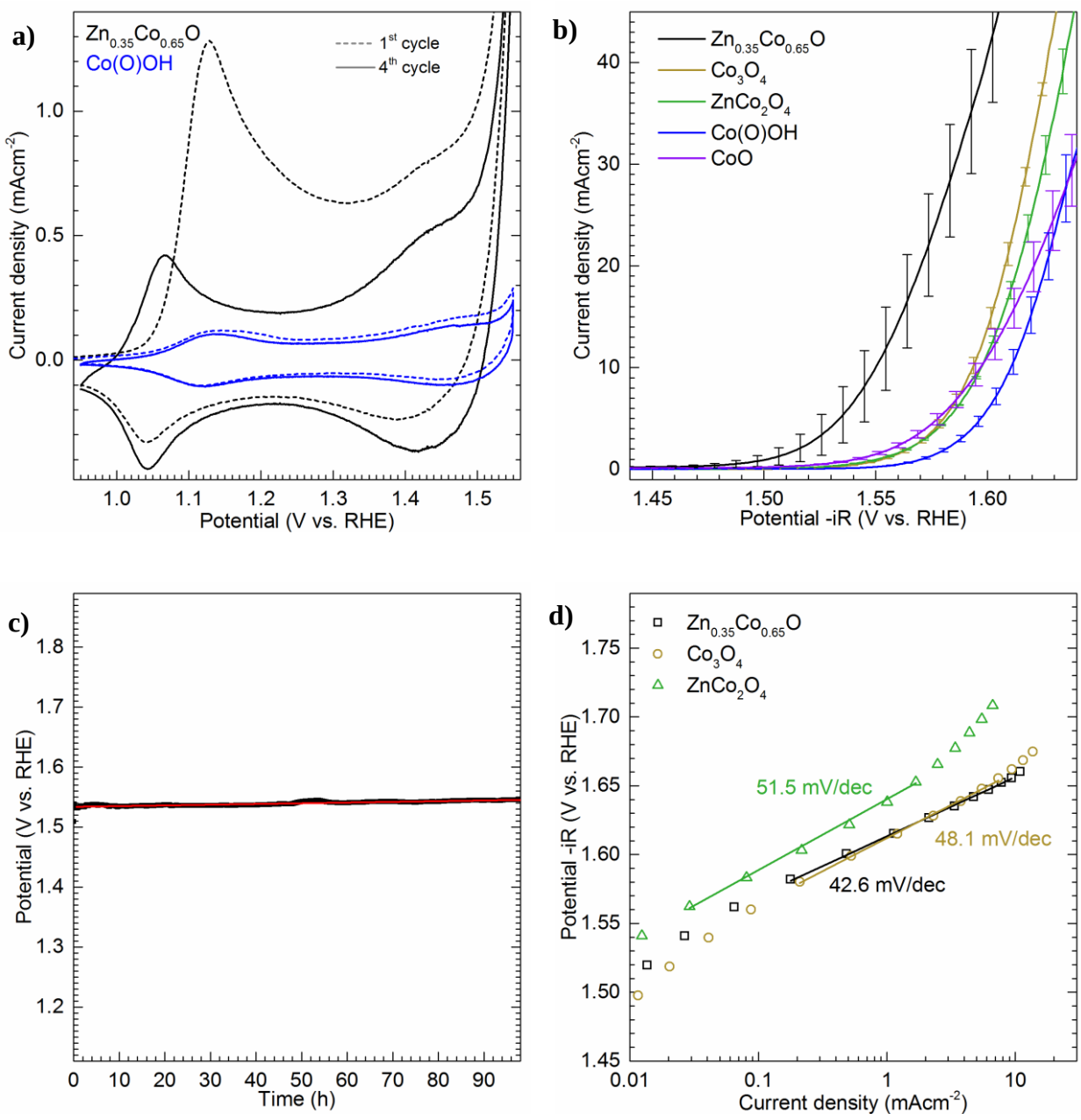

Figure 5. Cyclic voltammograms in 1 M KOH at a scan rate of 20 mVs^{-1} showing initial and 4th cycle of $Zn_{0.35}Co_{0.65}O$ and Co(O)OH (a). Averaged LSVs in 1 M KOH at a scan rate of 5 mVs^{-1} with error bars showing standard deviation: averaged overpotentials η towards the OER at 10 mA cm^{-2} are 322 mV for $Zn_{0.35}Co_{0.65}O$, 365 mV for Co_3O_4, 369 mV for $ZnCo_2O_4$, 382 mV for Co(O)OH and 369 mV for CoO (b). Variation of potential as function of time at a current density of 10 mA cm^{-2} in 1 M KOH on a gold screen-printed electrode. The potential at the beginning is

1.534 V vs. RHE, which corresponds to an overpotential η = 306 mV. Fitting the potential linearly, an increase of 0.12 mVh^{-1} can be reported (R^2 = 0.86) (c). Averaged Tafel plots of $Zn_{0.35}Co_{0.65}O$, Co_3O_4 and $ZnCo_2O_4$. The data were acquired in quasi-stationary conditions in 0.1 M KOH. Each potential was hold for 5 min, the current was averaged over this timeframe, and the Ohmic drop was determined using impedance spectroscopy (d).

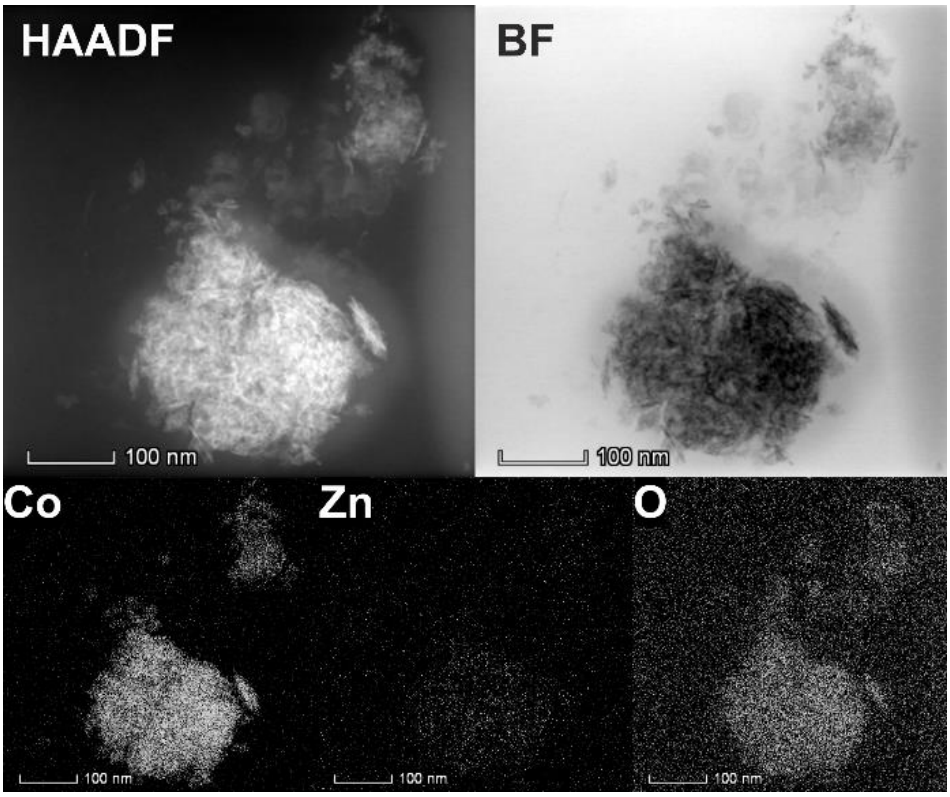

Figure 6. STEM HAADF and bright field micrographs and EDX mapping of cobalt, zinc and oxygen in $Zn_{0.35}Co_{0.65}O$ after the reaction: The cobalt-zinc ratio after 1 h electrochemical reaction is 93.5 % to 6.5 %.

8. Tables

Table 1. Comparison of electrochemical properties of different cobalt oxide based catalysts.

Catalyst	*ECSA* [cm²]	R_f [a)]	η [b)] [mV]	Tafel slope [c)] [mVdec^{-1}]
$Zn_{0.35}Co_{0.65}O$	21.93	310.18	322	42.6
Co_3O_4	0.91	12.81	365	48.1
$ZnCo_2O_4$	1.07	15.12	369	51.5
Co(O)OH	5.71	80.77	382	--
CoO	1.68	23.71	369	--

[a)]Roughness: *ECSA* divided by geometric area (7.069 mm^{-2}); [b)]at 10mA cm^{-2} in 1 M KOH;

[c)]measured in 0.1 M KOH under quasi-stationary conditions

Table 2. EDX Analysis of the Zn0.35Co0.65O before and after electrochemical reaction.

Sample	Co atom%	Zn atom%
before reaction	64.6 (±0.20)	35.3 (±0.17)
after reaction, bulk	94.5 (±0.14)	5.4 (±0.04)
after reaction, edge	97.4 (±0.34)	2.6 (±0.07)

9. TOC

Keyword: Structure-Property Relationships

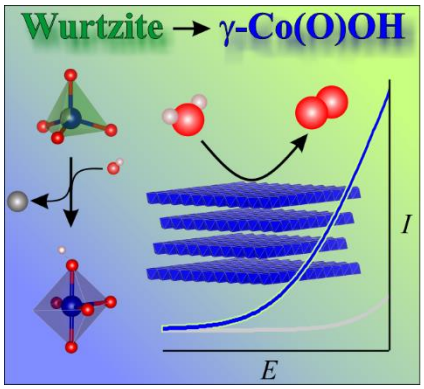

The precursor catalyst $Zn_{0.35}Co_{0.65}O$ is transformed *in situ* from the Wurtzite structure to the layered γ-Co(O)OH, while most of its zinc leaches out. This material shows outstanding catalytic performance and stability towards the OER in 1 M KOH (overpotential at 10 mA cm^{-2} $\eta_{initial}$ = 306 mV, $\eta_{98\ h}$ = 318 mV), based on coordinately unsaturated cobalt octahedra on the surface.